

EXPERIMENTAL AND COMPUTATIONAL LASER TISSUE WELDING USING A PROTEIN PATCH

Ward Small IV, Nicholas J. Heredia, Duncan J. Maitland, David C. Eder, Peter M. Celliers, Luiz B. Da Silva, Richard A. London, and Dennis L. Matthews

Lawrence Livermore National Laboratory, Livermore, California 94550

(Paper JBO-155 received May 19, 1997; revised manuscript received Sep. 22, 1997; accepted for publication Sep. 24, 1997.)

ABSTRACT

An *in vitro* study of laser tissue welding mediated with a dye-enhanced protein patch was conducted. Fresh sections of porcine aorta were used for the experiments. Arteriotomies were treated using an indocyanine green dye-enhanced collagen patch activated by an 805-nm continuous-wave fiber-delivered diode laser. Temperature histories of the surface of the weld site were obtained using a hollow glass optical fiber-based two-color infrared thermometer. The experimental effort was complemented by simulations with the LATIS (LAsEr-TISsue) computer code, which uses coupled Monte Carlo, thermal transport, and mass transport models. Comparison of simulated and experimental thermal data indicated that evaporative cooling clamped the surface temperature of the weld site below 100 °C. For fluences of approximately 200 J/cm², peak surface temperatures averaged 74°C and acute burst strengths consistently exceeded 0.14×10⁶ dyn/cm (hoop tension). The combination of experimental and simulation results showed that the inclusion of water transport and evaporative losses in the computer code has a significant impact on the thermal distributions and hydration levels throughout the tissue volume. The solid-matrix protein patch provided a means of controllable energy delivery and yielded consistently strong welds. © 1998 Society of Photo-Optical Instrumentation Engineers. [S1083-3668(98)00101-4]

Keywords collagen; infrared thermometry; modeling; surface temperature; tissue fusion.

1 INTRODUCTION

Laser tissue welding is a phrase used to describe the act of using laser light with or without extrinsic bonding materials such as protein solders or patches to join, seal, or appose biological tissues. Potential vascular applications include vessel anastomoses, aneurysm closure, and vessel wall reinforcement. Clinical experience has demonstrated the advantages of laser tissue welding over the conventional techniques of suturing and stapling: faster, reduced foreign body response (improved healing), and less susceptibility to leakage.¹ However, these advantages are tempered by a lack of reproducibly strong welds.

Extrinsic bonding media such as glues or solders and feedback control have been employed to combat the strength and repeatability issues currently affecting the developing practice of tissue welding.¹ The extrinsic agents provide a large surface area over which fusion with the tissue can occur, approximating tissue edges that eventually heal together in the days following laser treatment. In addition, incorporation of laser-absorbing chromophores enables localized surface heating

confined to the area of solder application, which reduces the extent of collateral thermal damage of the underlying tissue. Diagnostic feedback via surface temperature measurement has been used to control laser power delivery to achieve well-defined welding protocols en route to optimization.²⁻⁴

Although a diagnostic such as surface temperature is important for primary control of energy delivery, it does not reveal dynamic changes occurring below the tissue surface, where the weld actually occurs. This problem has been addressed by employing a numerical model of the laser-tissue interaction based on experimentally obtained surface temperature data.⁵⁻⁷ The combination of experiment and simulation enables characterization of the status of the tissue and the progression of the weld.

In this study, a laser-activated dye-enhanced collagen patch of uniform thickness was used to initiate repeatable repair of an arteriotomy *in vitro*, while a hollow glass optical fiber-based two-color infrared thermometer provided surface temperature data. The temperature histories were used in conjunction with the LATIS (LAsEr-TISsue) computer code to characterize the volumetric patch-

Address all correspondence to Ward Small IV. Tel: (510)423-2466; Fax: (510)424-2788; E-mail: small3@llnl.gov

tissue temperature distribution and hydration state. Consistent energy absorption of the uniform patch facilitated both the welding procedure and the subsequent computational analysis.

2 MATERIALS AND METHODS

2.1 TISSUE PREPARATION

Porcine hearts and the surrounding vasculature were freshly harvested (no rinsing during harvest) and kept refrigerated (5 °C) in sealed containers (not immersed in any fluid or wrapped in gauze) for 3 to 30 h prior to use. The aortas were dissected out within 1 h prior to welding. The arterial wall thickness was approximately 2 mm. The arteries were cut into approximately 3×3-cm slabs, and an incision 4 mm in length was made through the thickness of each slab. No gaps were observed between the edges of the incision. The slabs were soaked in phosphate-buffered saline (PBS) for several minutes to remove any blood and inhibit desiccation prior to welding. No stay sutures were used to appose the edges of the incision. The reason for using slabs rather than the innate tubular structure of the arteries is associated with the burst/leak pressure chamber used for strength assessment.

2.2 WELDING PROTOCOL

PBS-based 0.5-mm thick patches consisting of 70% weight by volume (w/v) porcine-derived gelatin (denatured collagen) and 0.25% w/v indocyanine green dye (ICG) were made by dissolving the gelatin and ICG in the PBS, applying heat to melt and form the gelatin mixture into 10×10×0.5-mm patches, and allowing them to cool and solidify. The gelatin comprised 41% of the total patch weight. The ICG was included to absorb the laser energy. In their final form, the patches were solid, but soft and pliable.

The tissue was placed on a glass substrate with the intima facing upward. A patch was placed over the incision on the intima to simulate an endovascular procedure as described by Glinsky, London and Zimmerman⁸ in which the patch surrounds a balloon at the end of a catheter. Laser energy from an 805-nm continuous-wave diode laser was delivered to the weld site via a 1-mm diameter fiber. The fiber tip was positioned 13 mm directly above the patch surface, yielding a Gaussian laser spot with a full-width at half-maximum (FWHM) of approximately 7 mm. The fiber was not moved during the irradiation. Though the center of the patch received a higher dose than the edges due to the Gaussian beam shape, the entire patch was irradiated. The laser delivered 1 W of power for 150 s, corresponding to an average fluence over the patch surface of approximately 200 J/cm² (power density ≈ 1.34 W/cm²), which allowed the patch to melt slightly and bond to the tissue surface. As a result of the thermally induced tissue shrinkage, the inci-

sion opened slightly, and some of the patch material melted into the incision during irradiation.

2.3 TWO-COLOR TEMPERATURE MEASUREMENT

The emissivity of a material may change as a function of temperature, chemical composition, and surface quality. Because the emissivity of the gelatin patch is unknown and may vary during the course of the welding procedure as a result of the water loss and melting caused by the temperature increase, a two-color method of temperature measurement was used. We assume the infrared emission of the protein patch is that of a gray body:

$$W = \epsilon \frac{2\pi hc^2}{\lambda^5} \frac{1}{e^{hc/\lambda kT} - 1} \quad [W \text{ cm}^{-2} \mu\text{m}^{-1}],$$

where W is the spectral emittance, ϵ is the emissivity (equal to 1 for a blackbody), h is Planck's constant, c is the speed of light, λ is the wavelength in microns, k is Boltzmann's constant, and T is the temperature in degrees kelvin. The spectral emittance of the target, and hence the signal yielded by a detector positioned to receive the emitted radiation, is dependent on two quantities: temperature and emissivity. If two detectors of different spectral bandpass are used to collect the emitted radiation, the ratio of the two signals can be calibrated using a blackbody of known temperature. Assuming that the emissivity of the sample is constant over the spectral bandpass of the system, the emissivity will cancel out of the ratio, making the calibration valid for any graybody target.⁹ Assuming the two signals originate from the same geometric region on the target, the ratio is also independent of the fiber-to-target distance in the case of a fiber-based system. It should be noted that the detected radiation actually contains ambient (room temperature) blackbody radiation and laser radiation reflected from the target (patch) surface in addition to the radiation emitted by the target itself. The intensity of the reflected blackbody radiation is scaled down by the surface reflectance, $1 - \epsilon$. Because the target in this study is water-based, its reflectance is low, and therefore the portion of the signals corresponding to reflected ambient radiation was negligible compared with the emittance of the much hotter target. Because the laser wavelength was not within the spectral bandpass of the fibers or detectors, any laser light reflected from the target surface was not detected.

An optical fiber-based two-color infrared thermometer was constructed to acquire patch surface temperatures during the course of the welding procedure. Radiation within a 1-mm diameter spot at the center of the laser spot was collected via two 700- μm hollow bore glass fibers^{10,11} directed to a common point on the patch surface, modulated by an optical chopper, and detected by two thermoelectrically cooled HgCdZnTe photoconductors of

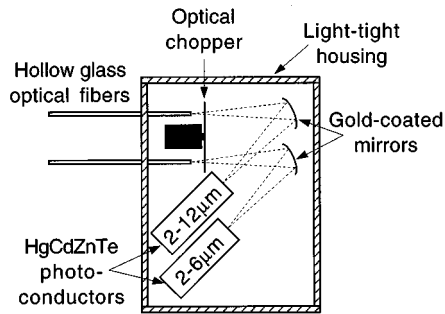


Fig. 1 The two-color infrared thermometry system in the laser tissue welding experiment. Radiation from the center of the laser spot is collected via two hollow glass fibers, modulated by a chopper, and transported to two detectors of different spectral bandpass. The modulated signals are recovered using lock-in amplification and sent to a computer for real-time temperature calculation.

different spectral response (2 to 6 μm and 2 to 12 μm , respectively). Lock-in amplifiers were used to recover the two modulated detector signals. The ratio of the signals was calibrated using a blackbody target (emissivity equal to 1) of known temperature varying from 20 to 125°C. The calibration formula was encoded into a computer for real-time temperature data acquisition. The configuration of the optical components is shown in Figure 1.

2.4 STRENGTH ASSESSMENT

Burst pressure was used to quantify the integrity of each weld immediately following completion of the welding procedure. Each artery slab was positioned in a pressure chamber so that the patched intima faced the inside to simulate actual blood flow. PBS was pumped into the chamber at a rate of 3 ml/min using a Harvard syringe pump. The pressures indicated by a pressure transducer connected to the chamber were recorded by a computer as a function of time. A diagram of the burst pressure measurement apparatus is shown in Figure 2. The burst pressure was noted as the highest (gauge) pressure reached, corresponding to the observed bursting of the weld. From the measured burst pressures, the

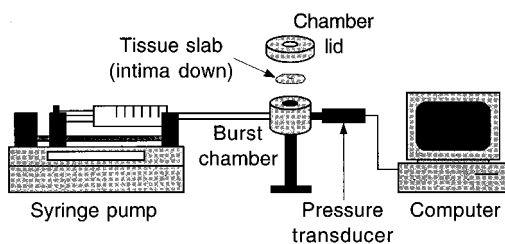


Fig. 2 Burst pressure measurement apparatus. The patched tissue slab is clamped (intima down) between the lid and body of the chamber, which is filled to the top with saline. Saline is infused into the chamber via a syringe pump at a rate of 3 ml/min until the weld bursts. A computer records the pressures measured by the pressure transducer as a function of time.

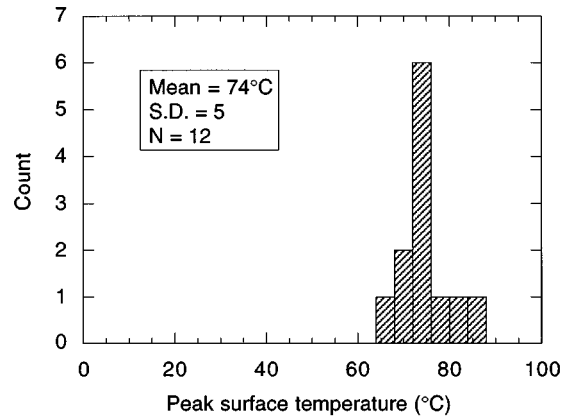


Fig. 3 Histogram of peak surface temperatures. The laser delivered 1 W (7-mm spot) for 150 s. The small variation in peak surface temperatures indicates that the absorption of laser energy was consistent among all trials. Part of the variation may have been due to error in the temperature measurement of $\pm 3^\circ\text{C}$.

hoop tension in the vessel wall was estimated using the law of Laplace that assumes a thin-walled membrane and spherical symmetry (the tissue bulged outward during the burst test, forming a hemisphere).

2.5 MODELING

The LATIS computer code simulated the exposure of the patched artery to near-infrared radiation using coupled Monte Carlo, thermal transport, and mass transport numerical models.^{6,7} LATIS was applied in a 2-D geometry with an experimentally measured Gaussian laser spot of 7 mm (FWHM) and an ICG-enhanced patch thickness of 0.5 mm, using the same laser power (1 W) and duration (150 s) as the experiment. The initial temperature was set to 25°C (room temperature) prior to laser exposure. The results of the simulations were compared with the temperature histories obtained in the laboratory to characterize the dynamic volumetric changes associated with laser irradiation.

3 RESULTS

3.1 THERMAL DYNAMICS

Peak surface temperatures of the patched artery at the center of the laser spot measured using the two-color infrared thermometer are shown in Figure 3. The peak surface temperatures of all trials were tightly clustered around 74°C. Figure 4 shows a typically experimentally measured temperature history of the patch surface at the center of the laser spot during the welding process and a corresponding simulation generated by LATIS. In both cases, after the laser is turned on, the temperature quickly rises and then begins to settle, eventually peaking in the neighborhood of 80°C. A sharp decrease in temperature occurs when the laser is turned off. Simulations generated for patched artery with

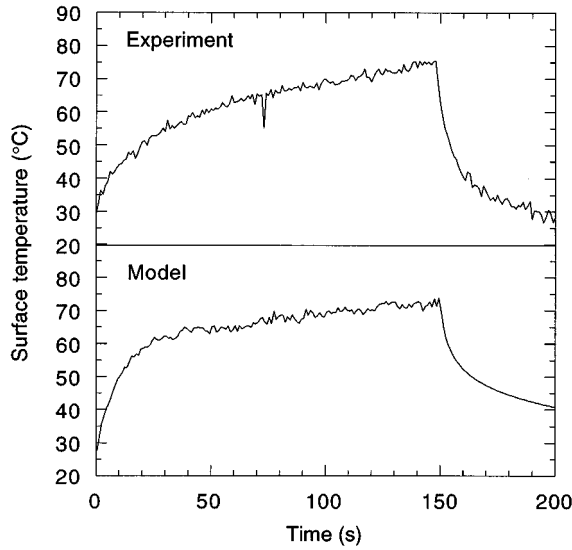


Fig. 4 Experimental and simulated temperature histories of the patch surface for 1 W of delivered laser power (7-mm spot). The laser is turned on at 0 s and turned off at 150 s. The noise in the simulation is due to the Monte Carlo laser transport model.

evaporation turned off resulted in a peak surface temperature of about 160°C (data not shown in figures), which is contradictory to the experiment.

LATIS was used to determine the energy-based effects beneath the patch surface. The simulated 2-D subsurface patch-tissue temperature distribution is shown in Figure 5. The highest temperature occurs beneath the patch surface, in the patch itself. Figure 6 shows the subsurface material density, which is related to the water content, plotted in two dimensions. Areas experiencing more water loss

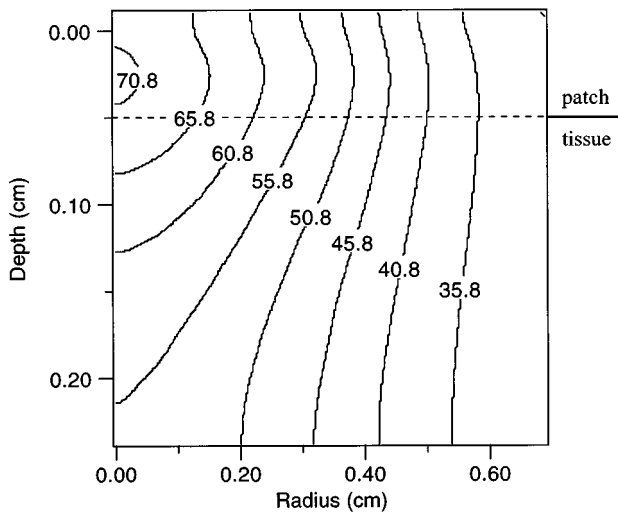


Fig. 5 Simulated subsurface temperature distribution of the patched artery at the time of laser shutoff. The contours are labeled in degrees Celsius. One watt of power (7-mm spot) was delivered for 150 s. The patch occupies the top 0.05 cm of the graph.

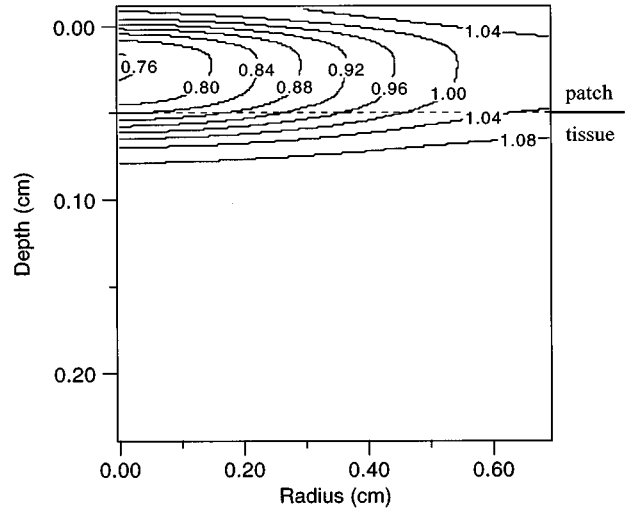


Fig. 6 Simulated subsurface density of the patched artery at the time of laser shutoff. The decrease in density corresponds to water loss. The contours are labeled in g/cm^3 . One watt of power (7-mm spot) was delivered for 150 s. The patch occupies the top 0.05 cm of the graph. The initial density of the patch was 1.15 g/cm^3 , and that of the tissue was 1.05 g/cm^3 .

have lower material densities. After the laser was turned off, the center of the patch lost approximately half of its water via evaporation, while the tissue was only slightly less hydrated than normal.

3.2 WELD STRENGTH

The acute hoop tension and corresponding burst pressure of the patched incisions are shown in Figure 7. For comparison, the hoop tension for the aorta in its natural cylindrical shape (important for an arteriotomy) was estimated to be $0.18 \times 10^6 \text{ dyn/cm}$ under physiologic conditions (120 mmHg blood pressure). The corresponding longitu-

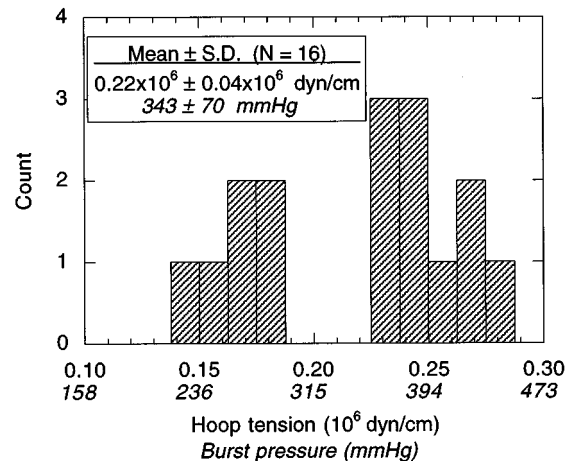


Fig. 7 Histogram of acute hoop tension and burst pressure (italics) for the patched incisions. The laser delivered 1 W (7-mm spot) for 150 s.

dinal tension (which is important for an end-to-end anastomosis) was estimated to be 0.09×10^6 dyn/cm. There appear to be two distinct groups around 0.17×10^6 dyn/cm and 0.25×10^6 dyn/cm, though no correlations were determined.

4 DISCUSSION

4.1 TEMPERATURE ACCURACY

The two-color infrared thermometer used in this study provided surface temperature data free from significant emissivity bias. The method of using the ratio of the signals automatically corrected for any emissivity effects, allowing recovery of more accurate surface temperatures. The accuracy of the technique in this study is slightly reduced due to error in the alignment of the two fibers to a common spot. This factor is important because the laser heats the surface nonuniformly, which could result in slightly different detected emittances for the two bands. According to the LATIS simulation in Figure 5, the surface temperature is nearly constant within a 2-mm-diameter circle at the center of the laser spot. Because the two fibers were aligned within this area of constant temperature, the accuracy of the measurement in this study was not significantly affected. The worst-case error is estimated to be within $\pm 3^\circ\text{C}$.

4.2 PATCH WELDING DYNAMICS

Experimental and simulated temperature histories indicated that evaporative cooling clamped the surface temperature of the patched tissue. This result agrees with previous studies.^{5,6,12} The patches provided sufficient hydration to allow evaporation to occur and prevented desiccation. The uniform thickness and composition of the patches resulted in consistent absorption of the laser energy, yielding only small variation in peak surface temperatures for a given laser fluence. It is possible that the shape of the surface temperature history could be controlled by changing the ICG and/or water concentrations in the patch and/or altering the laser power. Elimination of the problem of variability in solder thickness⁵ enabled repeatable energy delivery, which played an important role in coupling the experiment with the computer model, and may prove to be essential in determining welding protocols.

Agreement between the experimental and simulated surface temperatures allowed LATIS to predict subsurface energy-based changes. Temperature and hydration information beneath the tissue surface indicate the volumetric effects caused by the laser irradiation. The immediate area of the patch-tissue interface experienced significant ($\approx 25\%$) water loss due to evaporation. This loss may have resulted in the formation of electrostatic bonds, which, although acutely strong, will weaken when

sufficiently rehydrated.¹³ Exposure to the saline in the burst chamber did not immediately cause the patches to detach from the tissue surface, though it may have contributed to the eventual bursting of the weld.

4.3 WELD STRENGTH

The relatively high burst strength of the welds can be attributed to the strength of the collagen patch material as well as the patch-tissue bond. Observation of the patched incisions revealed that some of the patch material melted into the incision during laser irradiation, indicating that the strength lies in the patch-tissue fusion because direct tissue-to-tissue apposition between the edges of the incision was not achieved. This mechanism was used in previous patch welding studies.^{14,15} However, the patches used in this study would not be viable *in vivo* due to their solubility and low melting temperature. Sawyer¹⁴ noted a similar phenomenon when using gelatin-based solid-matrix materials for laser-assisted tissue welding. Whether the gelatin-based patches used in this study can be modified to compensate for these inadequacies is not known.

4.4 PATCHES IN PRACTICE

The use of patches facilitated the usually ambiguous tissue welding procedure, removing the commonly incurred need for a "trained eye." The end point for the procedure was marked by the slight but thorough melting of the patch; no subjective visual cues such as tissue blanching or shrinkage were necessary to achieve repeatable welds. Consistent laser energy absorption among the uniform patches resulted in reproducibly strong welds.

The clinical drawbacks of solubility and low melting temperature of these gelatin-based patches require further investigation. Incorporating additional constituents or increasing the laser power and/or duration to reach higher temperatures to alter the chemistry of the patches and redefine the final molecular and conformational state of the protein may help remedy these problems. At this time, the prospect of developing a physiologically compatible gelatin-based patch is not known. In addition, the clinical possibilities of residual blood in the welding field (particularly in the case of endovascular deployment) may influence the overall strength of the patch-tissue bond. Given the current clinical deficiencies of these patches, the concept of patch-mediated welding was demonstrated to address and overcome the ease-of-use and repeatability issues commonly associated with laser tissue welding.

Acknowledgments

This work was performed under the auspices of the U.S. Department of Energy by Lawrence Livermore National Laboratory under Contract W-7405-ENG-48 as part of the Cooperative Research and

Development Agreement TC-1085-95 with Conversion Energy Enterprises of Spring Valley, New York. The authors wish to thank J. Harrington for providing the hollow glass fiber, and J. Cox and K. Haney for their help in fabricating the experimental apparatus.

REFERENCES

1. L. S. Bass and M. R. Treat, "Laser tissue welding: a comprehensive review of current and future clinical applications," *Lasers Surg. Med.* **17**, 315-349 (1995).
2. S. D. Klioze, D. P. Poppas, C. T. Rooke, T. J. Choma, and S. M. Schlossberg, "Development and initial application of a real-time thermal control system for laser tissue welding," *J. Urol.* **152**, 744-748 (1994).
3. D. P. Poppas, R. B. Stewart, J. M. Massicotte, A. E. Wolga, R. T. V. Kung, A. B. Retik, and M. R. Freeman, "Temperature-controlled laser photocoagulation of soft tissue: in vivo evaluation using a tissue welding model," *Lasers Surg. Med.* **18**, 335-344 (1996).
4. R. B. Stewart, A. Benbrahim, G. M. LaMuraglia, M. Rosenberg, G. J. L'Italien, W. M. Abbot, and R. T. V. Kung, "Laser-assisted vascular welding with real-time temperature control," *Lasers Surg. Med.* **19**, 9-16 (1996).
5. W. Small IV, D. J. Maitland, N. J. Heredia, D. C. Eder, P. M. Celliers, L. B. Da Silva, R. A. London, and D. L. Matthews, "Investigation of laser tissue welding dynamics via experiment and modeling," *J. Clin. Laser Med. Surg.* **15**, 3-7 (1997).
6. D. J. Maitland, D. C. Eder, R. A. London, M. E. Glinsky, and B. A. Soltz, "Dynamic simulations of tissue welding," *Proc. SPIE* **2671**, 234-242 (1996).
7. R. A. London, M. E. Glinsky, G. B. Zimmerman, D. S. Bailey, D. C. Eder, and S. L. Jacques, "Laser-tissue interaction modeling with LATIS," *Appl. Opt.* **36** (1997).
8. M. E. Glinsky, R. A. London, and G. B. Zimmerman, "Computer modeling of endovascular patch welding using temperature feedback," *Proc. SPIE* **2623**, 349-358 (1996).
9. A. S. Tenney, "Radiation ratio thermometry," in *Theory and Practice of Radiation Thermometry*, D. P. DeWitt and G. D. Nutter, eds., Chap. 6, pp. 459-494, Wiley, New York (1988).
10. T. Abel, J. Hirsch, and J. A. Harrington, "Hollow glass waveguides for broadband infrared transmission," *Proc. SPIE* **2131**, 11-17 (1994).
11. T. Abel, J. Hirsch, and J. A. Harrington, "Hollow glass waveguides for broadband infrared transmission," *Opt. Lett.* **19**, 1034-1036 (1994).
12. J. H. Torres, M. Motamedi, J. A. Pearce, and A. J. Welch, "Experimental evaluation of mathematical models for predicting the thermal response of tissue to laser irradiation," *Appl. Opt.* **32**, 597-606 (1993).
13. J. Fenner, W. Martin, H. Moseley, and D. J. Wheatley, "Shear strength of tissue bonds as a function of bonding temperature: a proposed mechanism for laser-assisted tissue welding," *Lasers Med. Sci.* **7**, 39-43 (1992).
14. P. N. Sawyer, "Collagen welding rod material for use in tissue welding," U.S. Patent No. 5156613 (1992).
15. K. Sensaki, T. Arai, and S. Tanaka, "Laser patch welding: experimental study for application to endoscopic closure of bronchopleural fistula, a preliminary report," *Lasers Surg. Med.* **16**, 24-33 (1995).